ACS APPLIED MATERIALS & INTERFACES

Research Article

Cite This: ACS Appl. Mater. Interfaces 2019, 11, 26637−26647

www.acsami.org

Conjugation of a Small-Molecule TLR7 Agonist to Silica Nanoshells Enhances Adjuvant Activity

Ching-Hsin Huang,[†,∥] Natalie Mendez,[†,∥] Oscar Hernandez Echeagaray,[‡] Joi Weeks,[‡] James Wang,[†] Charles N. Vallez,[‡] Natalie Gude,[‡] William C. Trogler,[†] Dennis A. Carson,[§] Tomoko Hayashi,*[,§] and Andrew C. Kummel*[,†]

[†]Department of Chemistry & Department of Medicine, University of California, San Diego, 9500 Gilman Drive, La Jolla, California 92093-0358, United States

[‡]Molecular Biology Institute, San Diego State University, 5500 Campanile Drive, San Diego, California 92182, United States

[§]Moores Cancer Center, University of California, 9500 Gilman Drive, La Jolla, California 92093-0695, United States

Supporting Information

ABSTRACT: Stimulation of Toll-like receptors (TLRs) and/or NOD-like receptors on immune cells initiates and directs immune responses that are essential for vaccine adjuvants. The small-molecule TLR7 agonist, imiquimod, has been approved by the FDA as an immune response modifier but is limited to topical application due to its poor pharmacokinetics that causes undesired adverse effects. Nanoparticles are increasingly used with innate immune stimulators to mitigate side effects and enhance adjuvant efficacy. In this study, a potent small-molecule TLR7 agonist, 2-methoxyethoxy-8-oxo-9-(4-carboxybenzyl)adenine (1V209), was conjugated to hollow silica nanoshells (NS). Proinflammatory cytokine (IL-6, IL-12) release by mouse bone-marrow-derived dendritic cells and human peripheral blood mononuclear cells revealed that the potency of silica nanoshells-TLR7 conjugates (NS-TLR) depends on nanoshell size and ligand coating density. Silica nanoshells of 100 nm diameter coated with a minimum of ∼6000 1V209 ligands/particle displayed 3-fold higher potency with no observed cytotoxicity when compared to an unconjugated TLR7 agonist. NS-TLR activated the TLR7-signaling pathway, triggered caspase activity, and stimulated IL-1β release, while neither unconjugated TLR7 ligands nor silica shells alone produced IL-1β. An in vivo murine immunization study, using the model antigen ovalbumin, demonstrated that NS-TLR increased antigen-specific IgG antibody induction by 1000× with a Th1-biased immune response, compared to unconjugated TLR7 agonists. The results show that the TLR7 ligand conjugated to silica nanoshells is capable of activating an inflammasome pathway to enhance both innate immune-stimulatory and adjuvant potencies of the TLR7 agonist, thereby broadening applications of innate immune stimulators.

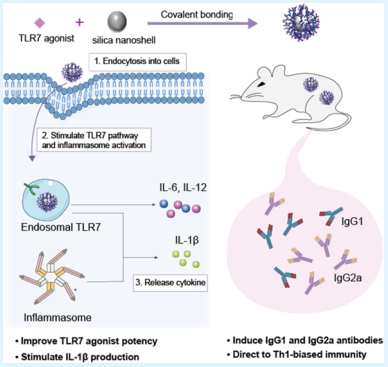

KEYWORDS: *nanoparticle, silica, TLR7, inflammasome, IL-1β, immune adjuvant, innate immunity*

INTRODUCTION

Nanoparticle technology has shown potential to improve immunotherapy. With tailored properties such as size, structure, surface chemistry, and drug-loading capacity, nanoparticles can increase the therapeutic index of immunostimulatory agents by facilitating entry into antigen-presenting cells (APCs)[1−3] and promoting local retention in the tissue.[4,5] The prolonged retention time can sustain a higher localized agent concentration that amplifies the immune response.[6] Employing nanoparticles in addition to immunostimulatory agents can also enhance and shape the immune responses toward a cellular- or humoral-biased immunity.[7−9] Cellular immunity that is mediated by T helper 1 cells (Th1) correlates to the induction of cytotoxic T cells to fight cancerous cells; humoral immunity that is mediated by T helper 2 cells (Th2) supports B cell proliferation to fight extracellular organisms.[10] Pattern recognition receptors (PRRs), such as Toll-like receptors (TLRs) and NOD-like receptors (NLRs), can activate the immune system and are commonly targeted when designing immunostimulatory agents.[11] TLR7 is one of the most extensively characterized TLRs for drug targeting.[12,13] For example, imidazoquinoline compounds produce proinflammatory cytokines, which display antitumoral and antiviral activities and are being investigated as cancer treatments.[14] NLRs, the other common target, including subfamily members such as NLRP1, NLRP3, and NLRP4, are important factors in the activation of caspase-1 in response to proinflammatory stimuli.[15] Despite promising specificity, these immunostimulatory agents exhibit insufficient immune response induction due to poor pharmacokinetics (PK) and thus require better formulation, such as conjugation to nanoparticles, to improve efficacy.[9,16]

Received: May 13, 2019
Accepted: July 5, 2019
Published: July 5, 2019

DOI: 10.1021/acsami.9b08295
ACS Appl. Mater. Interfaces 2019, 11, 26637−26647

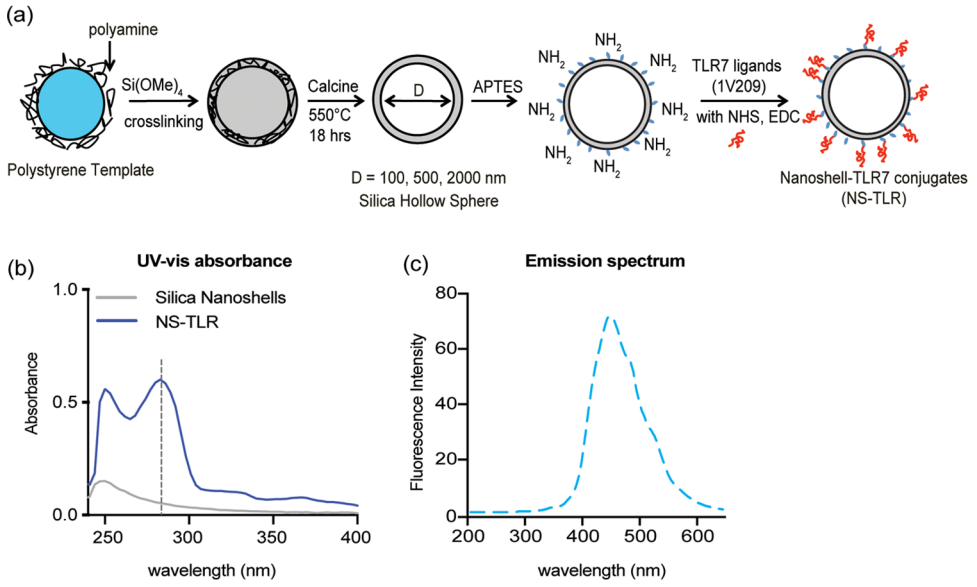

Figure 1. Synthesis and characterization of NS-TLR. (a) Synthesis and conjugation process of NS-TLR. (b) UV−vis absorbance spectrum of NS-TLR. (c) Fluorescence spectrum of NS-TLR with high coating density.

Silica nanoparticles have several advantages for immunotherapy, which include the ease of surface conjugation to a variety of immune-stimulants[17] and self-adjuvanticity. While other nanoparticles, such as polymers and lipids, have also been developed,[18,19] they have some limitations. Liposomes can improve PK;[20] however, their thermodynamic instability restrains their widespread use in a practical therapeutic setting.[21] Cholesterol insertion and PEGylation are used to improve liposome stability but may lead to decreased immune responses[22−25] or accelerated blood clearance,[26] respectively. Polymeric nanoparticles, commonly made of polylactic acid and polylactic-*co*-glycolic acid, are mostly compatible with soluble antigens, which are generally weak in immunogenicity and, therefore, may require the addition of commercialized adjuvants.[27] Problems with polydispersity and the requisite sophisticated manufacturing processes have also posed major challenges for reproducing a pharmaceutical-grade polymer−nanoparticle-based immunotherapy agent.[6,28,29] Conversely, silica nanoshells have the advantages of a well-established surface modification chemistry, a narrow size distribution, a highly tunable particle size, high stability in storage, and a high in vivo stability; therefore, they are a promising candidate to deliver immune-stimulants.[30] In addition, the hollow structure has shown to induce a more robust immune response compared to that of solid silica nanoparticles.[31,32] Several silica nanoparticle formulations have been reported to possess the self-adjuvanticity of being able to produce high titers of IgG antibodies comparable to the immune response induced by the commercial adjuvant alum.[33−35]

In the present study, immunostimulatory potencies of 100−2000 nm silica nanoshells conjugated with TLR7 agonists, termed nanoshell-TLR7 conjugates (NS-TLR), were investigated. Conjugation of TLR7 agonist (1V209) to 100 nm silica nanoshells at a high surface coating density significantly enhanced the agonistic potency compared to the unconjugated counterpart. Furthermore, silica nanoshells conjugated with TLR7 agonist stimulated IL-1β production through caspase activity, consistent with the silica nanoshells playing a vital role in immune stimulation. In vivo immunization studies using a model antigen showed that the NS-TLR enhanced Th1-biased cellular and humoral immune responses. These results demonstrate that the conjugation of a TLR7 agonist to silica nanoshells amplified the immune-stimulatory effects of the agonist, thereby broadening the potential agonistic application of these agents.

RESULTS AND DISCUSSION

Synthesis and Characterization of Silica Shells Conjugated to TLR7 Agonists. Hollow silica nanoshells were synthesized as previously described.[36] Synthesis and conjugation processes are depicted in Figure 1a. Nanoshells were modified with (3-aminopropyl)triethoxysilane (APTES) to functionalize the surface with a reactive primary amine group and, subsequently, conjugated to the carboxylic end of 1V209, which is a purine derivative TLR7 agonist.[37] The representative transmission electron microscopy (TEM) images in the Supporting Information, Figure S1a,b, illustrate that no morphological changes were observed after 1V209 conjugation to 100 nm nanoshells. The linkage between silica nanoshells and TLR7 ligand was confirmed by measuring the absorption of 1V209 at 283 nm on NS-TLR preparations. Additionally, NS-TLR fluoresces at 450 nm when excited with a wavelength of 283 nm (Figure 1c). This attribute enables convenient in vitro visualization without additional dye labeling to avoid potential influence on the interaction between nanoshells and cells.

Higher Ligand Density Increases TLR7 Activation of NS-TLR. The density of TLR7 ligands on carrier impacts functional outcomes of the conjugates.[8] To determine the influence of the ratio of nanoshells to 1V209, three different reactions were performed: (1) 0.084 mmol 1V209: 1 mg silica nanoshells reacted 2 h; (2) 0.017 mmol 1V209: 1 mg silica nanoshells reacted 2 h; and (3) 0.017 mmol 1V209: 1 mg silica nanoshells reacted 30 min. The amount of 1V209 conjugated to 100 nm nanoshells was quantified using UV−vis absorbance with a Rayleigh scattering subtraction (Figures S2 and S3). The absorbance spectra showed that a strong correlation between the initial concentration of 1V209 during conjugation

DOI: 10.1021/acsami.9b08295
ACS Appl. Mater. Interfaces 2019, 11, 26637−26647

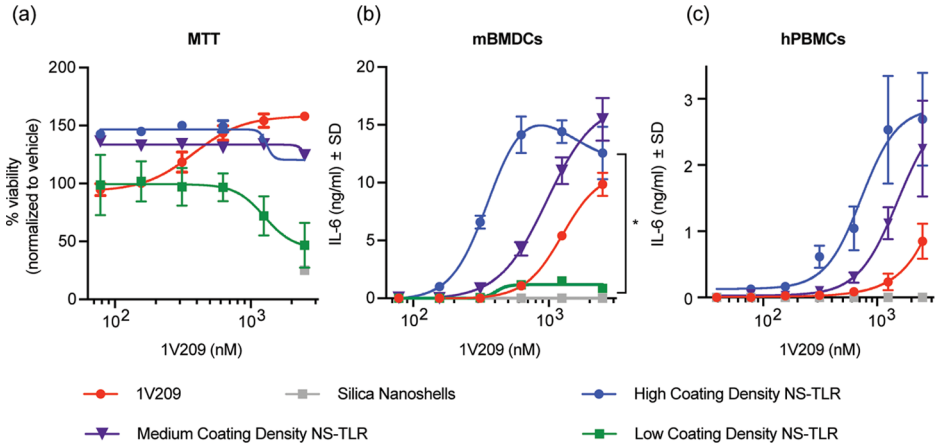

Figure 2. NS-TLR induces cytokine production and impacts viability in murine and human immune cells in a dose-dependent manner. Mouse BMDCs (10^5 cells) or human PBMCs (2×10^5 cells) were plated and incubated with serially diluted 100 nm NS-TLR at different coating densities for 18 h. (a) Cell viability in BMDCs for different coating density NS-TLR. Cell viability was measured by the MTT assay. IL-6 released in the culture supernatants of (b) mouse BMDCs or (c) human PBMCs incubated with unconjugated 1V209, high, medium, low coating density NS-TLR, and silica nanoshells. IL-6 cytokine was measured via ELISA. Cytotoxicity and cytokines were plotted by the concentration of TLR7 ligands that were equivalent to unconjugated 1V209. All data are representative dose−response curves in means ± SD and representative of three experiments. *$P < 0.05$ by two-way analysis of variance (ANOVA) with Tukey's post hoc analysis.

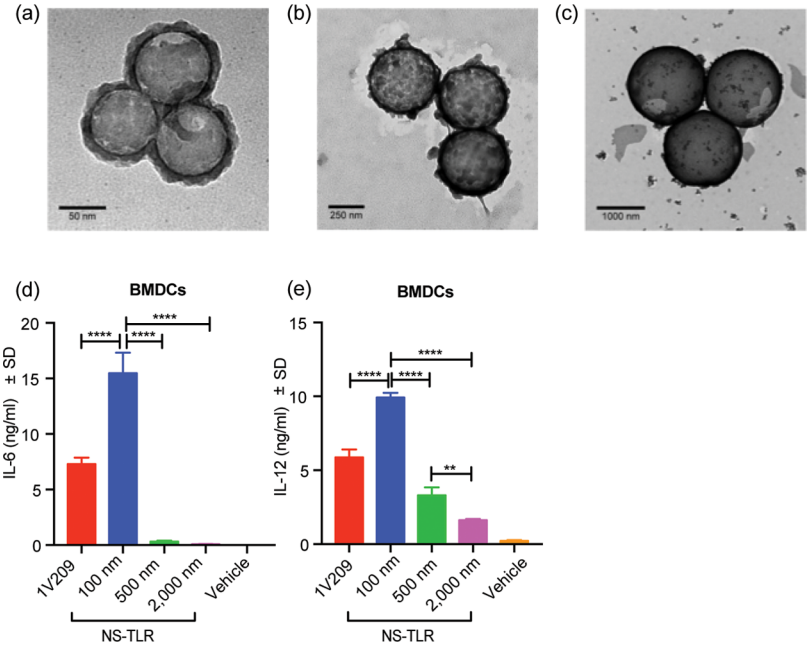

Figure 3. Characterization of silica nanoshells with 100, 500, and 2000 nm diameters. TEM images of (a) 100 nm, (b) 500 nm, (c) 2000 nm unmodified silica shells. Mouse BMDCs (10^5 cells) were plated and incubated with serially diluted NS-TLR with various sizes of particles for 18 h. (d) IL-6 and (e) IL-12 released in the culture supernatants of mouse BMDCs incubated with unconjugated 1V209, 1V209-conjugated 100, 500, and 2000 silica nanoshells. For all experiments, 1V209 = 2500 nM. The level of cytokines was measured by ELISA. All data shown are means ± SD of triplicates and representative of three independent experiments showing similar results. ** and **** denote $p < 0.01$ and $p < 0.0001$ by ordinary one-way ANOVA with Tukey's post hoc analysis, respectively.

and the final ligand density, 1V209, at the highest molar ratio (0.084 mmol 1V209: 1 mg silica nanoshells) for 2 h of reaction time yielded the highest density of 1V209 on the nanoshell surface. Nanoshells conjugated with less than 1000 1V209 ligands per nanoshell are defined as low-density NS-TLR, 1000−6000 1V209 ligands per nanoshells are defined as medium-density NS-TLR, and above 6000 1V209 ligands per nanoshell are defined as high-density NS-TLR (Supporting Information, Table S1).

Prior to testing the efficacy as a function of ligand coating, the effect of ligand density on cell viability was evaluated because previous reports have indicated that silica particles may induce apoptosis or necrosis in human immune cells and cancer cells.[38,39] An MTT viability assay was employed to assess the cytotoxicity of the NS-TLR in bone-marrow-derived dendritic cells (BMDCs) (Figure 2a). BMDCs were incubated with high-, medium-, or low-density NS-TLR, unconjugated 1V209, or silica nanoshells alone. Viability was normalized to the vehicle control (=100%). Medium- and high-density NS-TLR equivalent to 2500 nM TLR7 ligands yielded 96 and 100% viabilities, respectively. The silica nanoshells without conjugation only showed 26% viability. Since the silica toxicity

DOI: 10.1021/acsami.9b08295
ACS Appl. Mater. Interfaces 2019, 11, 26637−26647

is mainly derived from its bare surface,[40−42] the biocompatible 1V209 ligand coverage likely reduces the accessibility of silica surface, thereby mitigating the toxicity as the coating density increases. These data show that conjugation with 1V209 at medium and high coating densities counteracted the cytotoxicity of silica nanoshells alone.

A strong correlation was observed between ligand density and in vitro immune response. Downstream cytokines IL-6 and IL-12 were measured to assess dendritic cell (DC) activation. IL-6 and IL-12 can promote the differentiation of Th1 cells or cytotoxic T cells, which directly eliminate pathogens or cancerous cells.[43] The agonistic activity of the 1V209 ligand was enhanced in both human peripheral blood mononuclear cells (PBMCs) and mouse BMDCs treated with medium- and high-density NS-TLR (Figure 2b,c; Supporting Information, Figure S4). The half-maximal effective concentration (EC_{50}) and maximum effect (E_{max}) of the drug performance were quantified in Table S2 of the Supporting Information. High-density NS-TLR exhibited the lowest EC_{50} in both IL-6 and IL-12 readouts (279 ± 118 nM and 262 ± 20, respectively). The E_{max} of high-density NS-TLR is 1.5- and 3-fold higher than that of unconjugated 1V209 for IL-6 and IL-12 cytokine releases, respectively. As for the low-density NS-TLR, this formulation appeared to have a lower potency. These cumulative results indicate that high coating density NS-TLR using 100 nm nanoshells has the highest efficacy compared to unconjugated 1V209 and to the medium- and low-density coating NS-TLR.

Size of Silica Nanoshell Carriers Influences the Immune-Stimulatory Potency of NS-TLR. Previous studies demonstrate that innate immunostimulatory potencies of low-molecular-weight TLR7 ligands correlate with the size of drug carriers.[8] Such size-dependent immunomodulation can be attributed to various mechanisms such as particle internalization or intracellular distribution in DCs that interfere with maturation signaling.[44,45] Therefore, it is hypothesized that the size of silica nanoshells may influence the immune potencies of the TLR7 ligand−nanoshell conjugates. To test this hypothesis, 100, 500, and 2000 nm hollow silica nanoshells were synthesized, as previously described[36,46] (Figure 3a−c), and mouse BMDCs were treated with unconjugated 1V209, silica nanoshells, or NS-TLR of various sizes (100, 500, or 2000 nm).

Differently sized NS-TLR were incubated with BMDCs at 1V209 = 2500 nM. For these experiments, the absolute concentration of the 1V209 was kept constant, and all conjugates were with fixed coating ligands per area (high coating formula, summary shown in the Supporting Information, Table S1); therefore, the concentration of the silica shells was varied to maintain a constant 1V209 concentration. Silica nanoshells (100 nm) conjugated with 1V209 stimulated the highest cytokine release in BMDCs compared to 500 or 2000 nm silica nanoshells, as shown in Figure 3d,e. Since several viruses have diameters of about 100 nm,[47] the data was consistent with a 100 nm-sized NS-TLR, mimicking how pathogens are recognized by APCs and, therefore, enhancing the efficacy of the agonist. Silica nanoshells with a 100 nm diameter with high coating density demonstrated the most potent response and therefore were chosen for further studies.

NS-TLR Quickly Enters BMDCs and Specifically Stimulates TLR7 Signaling. TLR7, located at an endosomal compartment, signals through the MyD88 pathway and results in NF-κB activation, leading to proinflammatory cytokine (IL-6 and IL-12) release to drive DCs' maturation (Figure 4a). Therefore, the trafficking of NS-TLR into the endosomal compartment of DCs is important for the ligand to engage with the endosome in DCs where the TLR7 locates. Self-fluorescent properties of 1V209 were used to assess the internalization of NS-TLR in mouse BMDCs over time, using live imaging confocal microscopy. As shown in Figure 4b, NS-TLR associated with the cell membrane of BMDCs within 1 h and were trafficked into the cytosol compartment at 2 h post-treatment. By 6 h, the majority of NS-TLR localized in the late endosome/lysosome subcellular compartments. Collectively, these results showed that NS-TLR is readily taken up by DCs and accumulates in the late endosome/lysosome.

Following the confirmation of NS-TLR uptake by BMDCs, TLR7 agonist specificity was investigated in BMDCs derived from wild-type control (WT) and TLR7 knockout (TLR7KO) mice. Level of secreted proinflammatory cytokines IL-6 was used to assess TLR7-mediated NF-κB activation. Lipopolysaccharide (LPS), a TLR4 agonist, was used as a positive control. As shown in Figure 4c, the unconjugated 1V209, NS-TLR, and LPS induced IL-6 in the supernatant of WT BMDCs. However, IL-6 was not detectable in TLR7KO BMDCs treated with 1V209 or NS-TLR alone. Conversely, LPS produced IL-6 in TLR7KO BMDCs as it can still stimulate TLR4. These results demonstrated that TLR7 ligands conjugated onto silica nanoshells retain TLR7 specificity.

Combination of TLR Agonist and Silica Nanoshells Activates NLRP3 Inflammasome. The silica nanoshell alone or as a conjugate may enhance the immune response.[48] Several studies have reported that the phagocytosis of particulates results in the activation of NACHT, LRR, and PYD domain-containing protein 3 (NALRP3), a protein that acts as an intracellular PRR.[48−52] Upon activation, NALRP3 oligomerizes into a multiprotein complex containing NALRP3, caspase-1, and apoptosis-associated speck-like adaptor protein (shown as ASC in Figure 5e), which is commonly known as the NLRP3 inflammasome.[49] Such inflammasome regulates inflammatory cytokines such as IL-1β, activating the innate immune cells.[53,54] Inflammasome-mediated release of IL-1β in BMDCs requires two signals: TLR activation and NLR activation. Therefore, it was hypothesized that NS-TLR can modulate IL-1β production: silica nanoshells (NLR activator) trigger inflammasome complex formation concomitant with 1V209 (TLR7 activator)-signaling pathway activation. To test this hypothesis, BMDCs were treated with varying concentrations of NS-TLR, and IL-1β levels in the media were measured by ELISA as an indicator of inflammasome formation. As shown in Figure 5a, NS-TLR induced IL-1β production in a dose-dependent manner, whereas unconjugated 1V209 or silica nanoshells alone stimulated negligible IL-1β release. Previous studies showed that pure TLR agonists induced IL-1β secretion when there were existing NLRP3 stimuli in the cells such as mitochondrial dysfunction-derived signal, adenosine 5′-triphosphate (ATP), nigericin, etc.[55,56] In the present study, pure 1V209 (TLR7 agonists) did not induce IL-1β secretion because 1V209 alone did not have NLRP3 stimuli (silica nanoshells) to stimulate the NLRP3 pathway and transform pro-IL-1β into releasable IL-1β. Treating cells with a mixture of unconjugated silica nanoshells and unconjugated 1V209 resulted in a similar level of IL-1β release to that seen with NS-TLR treatment (Supporting Information,

DOI: 10.1021/acsami.9b08295
ACS Appl. Mater. Interfaces 2019, 11, 26637−26647

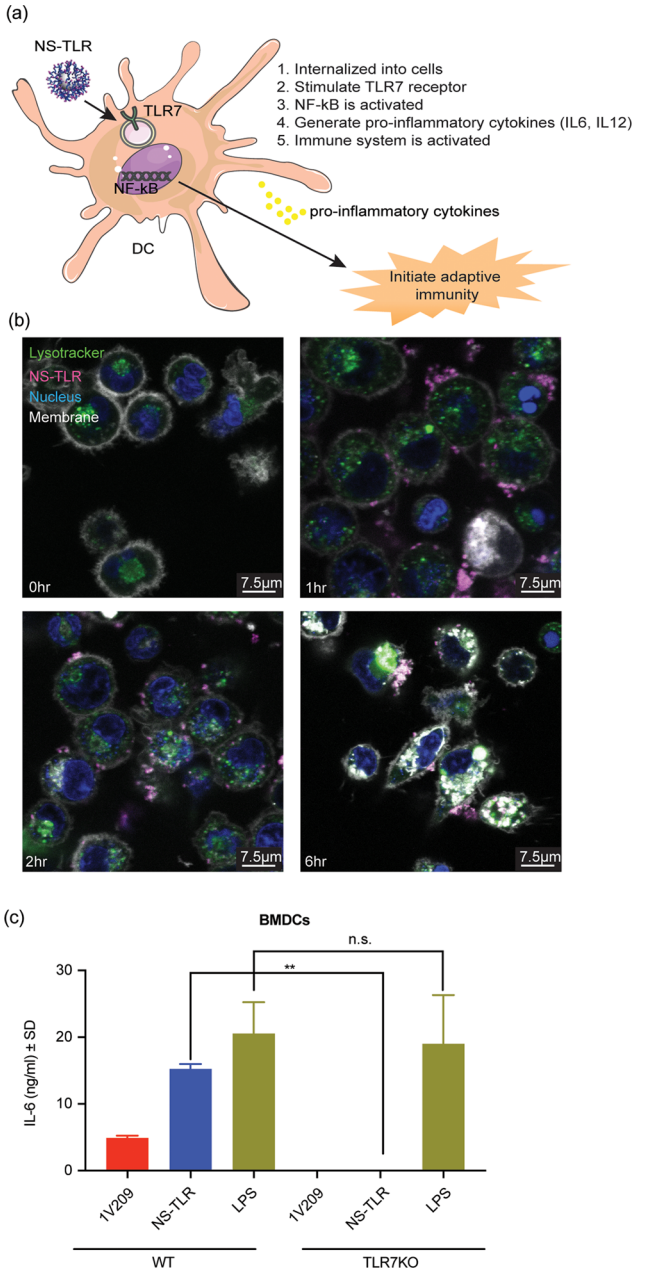

Figure 4. NS-TLR enters the endosome compartment of mouse BMDCs. (a) Illustration of NS-TLR targeting TLR7 located in the endosomal compartments stimulating proinflammatory cytokine production and enhancing the immune response. (b) Mouse BMDCs were incubated with NS-TLR (pink) for up to 6 h. Live cell dyes for the late endosome/lysosomes (lysotracker, green), nuclei (DAPI, blue), and membrane (membrane mask, white) were added 5−30 min prior to acquisition. Images were acquired 1, 2, and 6 h post-treatment. Untreated BMDCs served as the 0 h negative control. NS-TLR progresses from the media, through the membrane, into the cytoplasm, and eventually resides in the late endosome/lysosome of the cell. (c) Unconjugated 1V209 (1250 nM), NS-TLR (1250 nM), and 100 ng/mL LPS (TLR4 agonist) were incubated with wild-type or TLR7-deficient BMDCs. Secreted IL-6 protein levels were measured by ELISA. All data shown are means ± SD and representative of three independent experiments showing similar results. **** denotes $p < 0.0001$ by ordinary one-way ANOVA with Bonferroni post hoc.

Figure S5). These results suggest that IL-1β production is dependent on two signaling pathways triggered by the presence of both 1V209 and silica nanoshells but does not require conjugation or cotrafficking through the cells.

To verify that IL-1β release was TLR7-dependent, NS-TLR were incubated with TLR7 knockout (TLR7KO) BMDCs. TLR7KO BMDCs treated with NS-TLR failed to release IL-1β, indicating that IL-1β release requires TLR7 activation (Figure 5b). The mechanism of pro-IL-1β to IL-1β conversion was also verified. Pro-IL-1β is an inactive form and requires caspase to proteolytically cleave and generate releasable IL-1β; therefore, WT BMDCs were incubated with a pan-caspase inhibitor, carbobenzoxy-valyl-alanyl-aspartyl-[*O*-methyl]-fluoromethylketone (Z-VAD-FMK), to assess whether NS-TLR-mediated IL-1β release was caspase-1-dependent. Caspase inhibition blocked IL-1β release in NS-TLR-treated cell (Figure 5c), while IL-6 release was refractory to the presence of Z-VAD-FMK (Figure 5d). These results indicate that caspase-meditated inflammasome activation by both silica nanoshells and TLR7 activation leads to IL-1β release, and the induction of proinflammatory cytokines IL-6 was independent of caspase-inflammasome activation.

Figure 5e depicts a hypothetical mechanism of action by which NS-TLR stimulates the innate immune response. Table S3 shows a summary of reported studies of silica nanoparticle-induced IL-1β. The data suggested that these NS-TLR can improve the pre-existing innate immune-stimulatory agents and trigger IL-1β production without the need for prepriming cells, while existing nanoparticles require an extra step of prepriming cells (Table S3). A two-pronged pathway is proposed for NLRP3 inflammasome activation in DCs: the first signal is triggered by 1V209 to generate NALP3 and pro-IL-1β production through the activation of NF-κB, while the second signal is triggered by silica nanoshells. The data are consistent with 1V209 triggering the NF-κB pathway and producing pro-IL-1β (inactive form), while silica nanoshells stimulate the formation of the NLRP3 inflammasome, which cleaves pro-IL-1β into IL-1β (active form) for release. The inflammasome/IL-1 pathway represents a potential therapeutic target for developing novel cancer treatments in responsive tumor types.[57,58]

NS-TLR Enhances Cellular and Humoral Immune Responses. Conjugation of TLR7 ligands onto silica nanoshells can enhance the in vitro potency of TLR7 agonistic activity and IL-1β production, and silica nanoshells can support prolonged local depot effects that may enhance immune-stimulatory effects when translating to in vivo studies.[59] Therefore, an immunization model using ovalbumin (OVA) was performed to study the effects of NS-TLR on the in vivo immune response. IgG2a and IgG1 were used as indicators for Th1-type and Th2-type immune responses, respectively.[60] The Th1-type response, regulating cellular immunity, contributes to the development and activation of cytotoxic T cells. Conversely, Th2-type immunity regulates the humoral immune response and induces the proliferation and differentiation of B cells. Th1-type immunity is critical for cancer immunotherapy and virus elimination, while Th2-type immunity is critical for body protection against parasite infection.[10,61] Five groups (n = 3−4) of mice were immunized with OVA plus (1) silica nanoshells alone, (2) 1V209 alone, (3) mixture of 1V209 and nanoshells without conjugation (Mix.), (4) NS-TLR, and (5) vehicle as a negative control. The simple mixture of silica nanoshells and 1V209 without covalent

DOI: 10.1021/acsami.9b08295
ACS Appl. Mater. Interfaces 2019, 11, 26637−26647

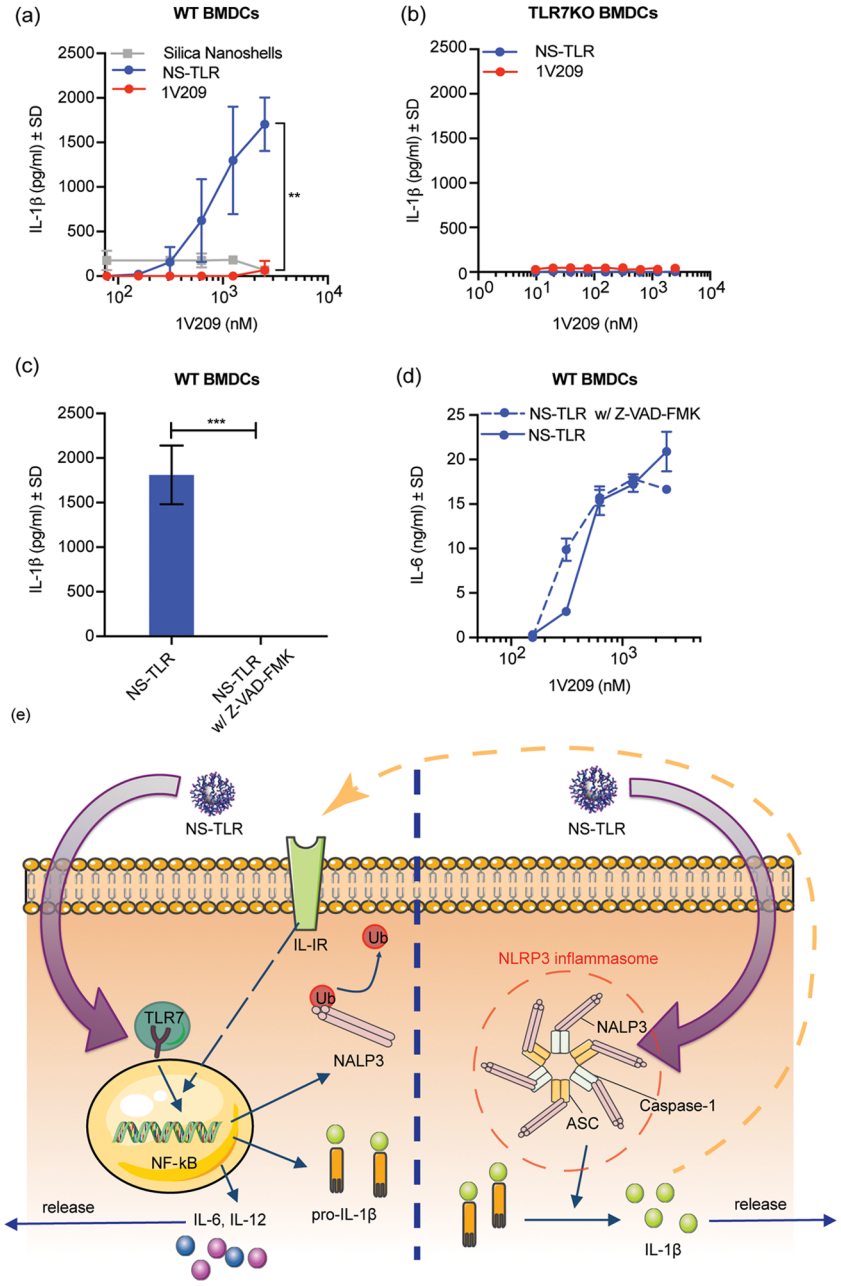

Figure 5. NS-TLR induces IL-1β release in BMDCs. NS-TLR (75−2500 nM, high coating density), unconjugated 1V209, and silica nanoshells were incubated with BMDCs for 18 h. IL-1β induction in (a) wild-type BMDCs and (b) TLR7-deficient BMDCs. NS-TLR (2500 nM) were incubated with wild-type BMDCs in the presence of pan-caspase inhibitors (Z-VAD-FMK), and (c) IL-1β and (d) IL-6 inductions were measured. All cytokines were measured by ELISA. All data shown are means ± SD in triplicates. Dose−response curve was analyzed by one-way ANOVA with Dunn's multiple comparison test. (e) Current working hypothesis of the mechanism of TLR7 signaling and NLRP3 pathway induced by NS-TLR.

bonds was evaluated at the same time to assess whether the linkage between TLR7 ligands and nanoshells is needed to have desirable pharmacokinetics. The mice were immunized as protocol shown in Figure 6a. Antibody production in sera is shown in Figure 6b,c.

NS-TLR (covalent bond) enhanced both IgG2a and IgG1, while unconjugated 1V209 or vehicle-treated groups showed nearly zero IgG2a (Th1 response) production as measured by ELISA. NS-TLR treatment showed an approximately 1000-fold increase in OVA-specific IgG2a antibodies compared to silica nanoshells or the mixture of 1V209 and silica nanoshells. Unconjugated 1V209 did not enhance IgG2a production, possibly due to rapid clearance from the injection site because of the undesirable pharmacokinetics of low-molecular-weight drugs. No synergistic effect on IgG2a production was observed in samples treated with unconjugated silica nanoshells and free 1V209 (Mix.). These results indicated that simultaneously activating the two pathways was not sufficient to generate a strong Th1 immunity. Because the antigen-specific IFN-γ response indicates the induction of the Th1-type immunity, IFN-γ production was measured in splenocytes isolated from treated mice. Consistent with the trends observed in Th1-type cellular responses, treatment with NS-TLR stimulated higher antigen-specific IFN-γ release by splenocytes (Supporting Information, Figure S6).

DOI: 10.1021/acsami.9b08295
ACS Appl. Mater. Interfaces 2019, 11, 26637−26647

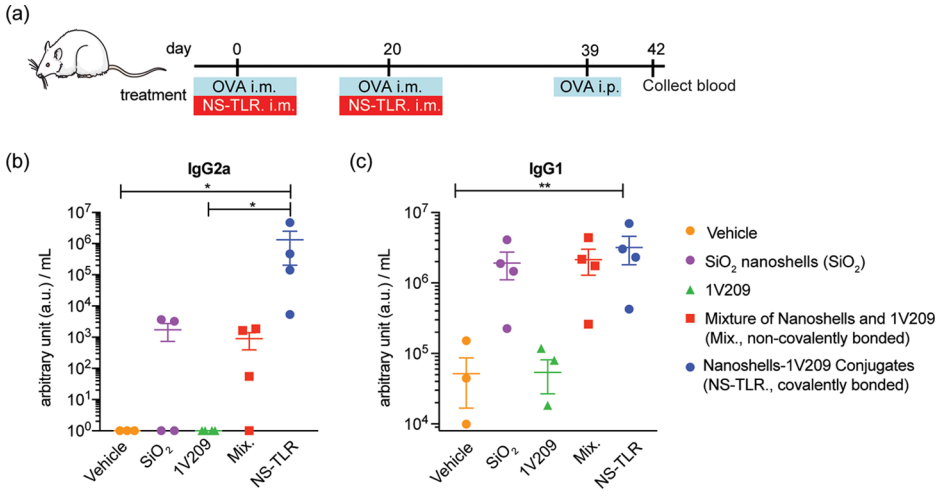

Figure 6. Immunization study of NS-TLR with OVA as a model antigen. (a) Balb/c mice (n = 3−4) were intramuscularly immunized with chicken OVA and NS-TLR, unconjugated 1V209 mixed with silica nanoshells (Mix.), silica nanoshells or unconjugated 1V209 alone on days 0 and 20 and sacrificed on day 42. Serum levels of (b) anti-OVA IgG2a and (c) IgG1 measured by ELISA are shown as mean ± SEM. Data were analyzed with Kruskal−Wallis one-way ANOVA with Dunn's post hoc analysis. * denotes $p < 0.05$ and ** denotes $p < 0.01$.

Levels of OVA-specific IgG1 antibodies were increased in all treatments containing silica nanoshells (Figure 6c), which suggests that silica nanoshells can enhance Th2-type response but covalent bonding between TLR7 agonists and nanoshells is required for the induction of Th1-type immune response. The mechanism of silica self-adjuvants is probably similar to that of the commercial adjuvant, alum, that activates the immune system through NLRP3 inflammasome formation.[62] However, alum is limited to a Th2-type response enhancement and fails to elicit an equally efficacious Th1 response.[63,64] Some studies have used TLR7 agonists adsorbed onto commercialized adjuvant, alum, to improve adjuvanticity.[65] Since alum is neurotoxic and may damage the blood−brain barrier, there are serious concerns.[66] In the present study using silica nanoshells as the delivery platform of TLR7 agonists, the potential toxicity of silica particle is mitigated by the free surface coverage. The MTT assay (Figure 2c) that measured the metabolic activity to model the cell toxicity showed that the higher coverage (higher 1V209 ligand per nanoshell) silica nanoshells displayed lower cytotoxicity, which is likely due to 1V209 ligand blocking the free silica surface. This is consistent with previous reports that the surface generation of reactive oxygen species is the main source of silica toxicity.[41] 1V209 is a small-molecule drug that has undesired properties, such as fast clearance after administration. As shown in Figure 6b,c, unconjugated TLR7 agonists (1V209) demonstrated a quiescent adjuvant activity as shown in the low induction of IgG2a and IgG1. These results implied that unconjugated TLR7 agonist small molecules (1V209) cleared away relatively rapidly from the injection site and thus failed to induce a robust immune response. A table summarizing previous studies using silica nanoparticles as adjuvants is shown in Table S4. In summary, small-molecule drug TLR7 agonists cannot be retained locally to continuously stimulate the TLR7-signaling pathway. Conjugation, however, was able to lengthen the retention time of small-molecule agonists, leading to continuous recruitment of APCs and sustained stimulation in situ. Localizing 1V209 largely benefits the efficacy of this small-molecule TLR7 agonist drug. These data together with our in vitro studies implied that the TLR7 ligand−nanoshell conjugates induced both inflammasome-dependent IL-1β and inflammasome-independent proinflammatory cytokines that enhanced the function of APC and induced the desirable antigen-specific Th1-biased immune responses.

CONCLUSIONS

The present study has shown that the immune potency of small-molecule TLR7 ligands was amplified when conjugated to silica nanoshells while retaining the ligand−receptor specificity. The amplification is both particle-size-dependent and ligand-density-dependent, where high-density-coated 100 nm silica nanoshells showed the greatest agonistic activities in vitro. The increased coverage of TLR7 ligands on silica nanoshell surfaces mitigated the cytotoxicity of the bare silica nanoshells and improved the therapeutic effect. The NS-TLR enhanced both TLR7 signaling and induced the activation of the NALP3 inflammasome to achieve a more robust immune response. The induction of proinflammatory cytokines IL-6 and IL-12 was refractory to the caspase inhibitor, which indicates that the induction of these cytokines was solely TLR7-dependent and -independent of caspase-inflammasome activation. Silica nanoshell conjugation also resulted in the lengthening of the local drug retention time to maximize drug effects. More APCs infiltrate to the administrated site, continuously activate maturation, and strengthen the subsequent immune response. Based on the in vivo vaccination study, antigen-specific immune response was displayed and successfully amplified by NS-TLR for both Th1-type and Th2-type immune responses. The dual enhancement implies a broader application as vaccine adjuvants or even as monotherapy for cancer treatment. These results suggested that conjugates could be used in cancer treatment as monotherapy or as a candidate for combinatorial synergistic delivery.

METHODS

Materials. *N*1-(3-Trimethoxysilylpropyl)diethylenetriamine (DETA, Cat. No. D93856), tetramethyl orthosilicate (TMOS), trimethoxy(phenyl)silane (TMPS), (3-aminopropyl)triethoxysilane (APTES), *N*-hydroxysuccinimide (NHS, Cat. No. 130672), *N*-(3-dimethylaminopropyl)-*N*′-ethylcarbodiimide (EDC), and solvents were purchased from Sigma-Aldrich (St. Louis, MO). Polystyrene

DOI: 10.1021/acsami.9b08295
ACS Appl. Mater. Interfaces 2019, 11, 26637−26647

templates (100−2000 nm) were purchased from Polysciences Inc. (Warrington, PA). 4-[6-Amino-2-(2-methoxyethoxy)-8-oxo-7*H*-purin-9(8*H*)-yl]methylbenzoic acid (1V209) was synthesized as previously described.[37] RMPI medium 1640 (Cat. No. 11875-093, Gibco, Thermo Fisher Scientific, Waltham, MA) was supplemented with 10% fetal bovine serum (Cat. No. 35-011-CV, Corning Inc., Corning, NY), 100 U/mL penicillin, 100 μg/mL streptomycin, and 292 μg/mL glutamine (Cat. No. 10378-016, Life Technologies, Carlsbad, CA) to prepare the complete media (RP-10). Pan-caspase inhibitor, Z-VAD-FMK, was purchased from Invivogen (Cat. No. tlrl-vad, San Diego, CA).

Instrumentation. TEM images were captured using a JEOL 1400 electron microscope. UV−vis absorption was measured with a NanoDrop ND-100 spectrophotometer (Wilmington, DE) and infinite M200 plate reader (TECAN, Mannedorf, Switzerland).

ELISA Reagents. Mouse anti-IL-6 antibodies (Cat. Nos. 554400 and 554402), mouse anti-IL-12 antibodies (Cat. Nos. 551219 and 554476), and recombinant mouse IL-6 and IL-12 standards (Cat. Nos. 554582 and 554594) were purchased from BD Pharmingen (Franklin Lakes, NJ). Tetramethylbenzidine (TMB) was used as a substrate for HRP. Mouse IL-1β (Cat. No. DY401) and IFN-γ (and DY485) ELISA kits were purchased from R&D System (Minneapolis, MN). Chicken ovalbumin (OVA, Cat. No. LS003049) was purchased from Worthington (San Diego, CA) and IgG1-AP goat antimouse antibody (Cat. No. 1070-04) and IgG2a-AP goat antimouse (Cat. No. 1080-04) antibody were purchased from Southern Biotech (Birmingham, AL). *p*-Nitrophenyl phosphate tablet (*p*NPP) was purchased from Sigma-Aldrich (Cat. No. 2700, St. Louis, MO).

Synthesis of 100 nm Nanoshells. A 0.2% DETA solution was prepared in ethanol and quickly vortexed. Ethanol (430 mL), 40 mL of 0.2% DETA solution, 2.5 mL of water, and 6.25 mL of 100 nm polystyrene beads (2.5% solids (w/v) aqueous suspension) were mixed and stirred for an hour at 4000 rpm. Polystyrene beads (100 nm) were used as templates for synthesizing silica nanoshells. DETA was physically adsorbed onto polystyrene beads and generated a positive surface charge during initial nucleation of the polycondensation polymerization. Silica precursor was prepared by suspending 375 μL TMOS and 500 μL TMPS in 4 mL of ethanol and briefly vortexed. This precursor solution was added to the polystyrene beads/DETA solution and stirred for 5 h at 4000 rpm. The TMOS formed silicic acid and its various deprotonated forms, which interacted with positive charges on the surfaces of the beads to propagate polymerization. After 5 h, samples were centrifuged at 3200 rpm for 25 min and washed twice with ethanol. Samples were left to dry overnight and calcined at 550 °C (ramping at 5 °C/min and soaked at 550 °C for 5 h). The synthesis reaction yields 80−100 mg hollow 100 nm silica nanoshells. Different sizes of hollow silica shells were synthesized with similar methods that were reported in previous studies (Figure S7).[36,67]

1V209 Linking Chemistry and Quantification. 1V209 was synthesized as previously described.[37] NHS, EDC, and 1V209 were prepared at 10 mg/mL in anhydrous DMSO. A 1:1:1 molar ratio of NHS, EDC, and 1V209 was mixed and pulse-vortexed for 2 h at 3200 rpm to form a 1V209 solution (1×). Meanwhile, silica nanoshells were amine-functionalized as follows. The silica nanoshells were suspended in DMSO at 2.5 mg/mL, vortexed, and sonicated until the nanoshells were well suspended. APTES solution (2 μL of 10%) was added per mg of silica and pulse-vortexed for 2 h at 3200 rpm. After 2 h, nanoshells were centrifuged at 4000 rpm for 10 min, washed twice with 4 mL of DMSO, and resuspended at 20 mg/mL in anhydrous DMSO. Diluted 1V209/NHS/EDC solution (110 μL, 0.5× or 0.01×) was added to silica nanoshells per mg of nanoshells and corresponded to high- or medium-density coating formulation, respectively. For low-density formulations, the volume of diluted 1V209/NHS/EDC (0.01×) added to nanoshells was kept constant, but the reaction time was reduced to 30 min. All conjugates were washed twice as before and reconstituted at 20 mg/mL based on silica nanoshell mass for further characterization. To calculate the number of ligands, a standard curve was created using serial dilutions of known concentrations of 1V209. 1V209's peak absorbance at 283 nm was used to interpolate the number of TLR7 ligands conjugated per nanoshell, which was subsequently converted to the total number of ligands in the solution. Correction for scattering by the nanoshells was needed for nanoshell structure. Inner light scattering caused by the incident light interacting with the hollow nanoshell wall and passing through the interior filled with a culturing medium may be amplified by the difference in refractive indices between the solid wall and the culturing medium. Aggregates or colloids present in the nanoshell suspension also scatter light elastically from the solution. This effect, known as Rayleigh scattering, creates high background interference at the blue end of the absorption spectrum.[68] Hence, a Rayleigh scattering curve-fitting proportional to λ^{-4} was applied to perform the baseline subtraction, and the number of ligands per nanoshell was quantified after scattering background subtraction. Note that by using blank silica nanoshells to estimate the light-scattering effect, it provided a reasonable baseline correction for the ligand absorbance measurement. However, nanoparticle aggregation and self-quenching (if measuring fluorescence) may also impact the accuracy of surface concentration estimation.[69]

Animals. Female Balb/c and C57BL/6 mice (6−8 weeks old) were purchased from The Jackson Laboratory (Bar Harbor, ME) and from Charles River Laboratories (Wilmington, MA) for in vivo and BMDC isolation. Mice genetically deficient for TLR7 were kindly gifted from Dr Shizuo Akira (Osaka University, Osaka, Japan) and maintained by the University of California San Diego Animal Care Program. All procedures and protocols were approved by the UC San Diego Institutional Animal Care and Use Committee.

In Vitro Cytokine Induction in mBMDCs and hPBMCs. Murine BMDCs from C57BL/6 mice or human PBMCs isolated from buffy coats obtained from the San Diego Blood Bank (San Diego, CA) were prepared as described previously.[70] mBMDCs and hPBMCs were plated in a 96-well plate at 1×10^5 or 2×10^5 cells/well (150 μL), respectively. Unconjugated 1V209, NS-TLR, or silica shells were serially diluted in DMSO and diluted further with RP-10 at a final DMSO concentration of 0.5%. After incubating 18 h at 37 °C under 5% CO_2, the supernatants were collected and the levels of cytokines (IL-6, IL-12, and IL-1β) were determined by ELISA.

In Vitro Intracellular Tracking of NS-TLR in APCs. BMDCs were plated at a density of 6×10^5 cells/well in #0 cover glass 24-well plates (In Vitro Scientific, Noble Park North, Australia) with RP-10 at 37 °C. The cells were treated with NS-TLR at a 1 μM 1V209 equivalent concentration or vehicle control. Samples were stained with lysotracker green (65 nM, Thermo Fisher Scientific) for the late endosome/lysosomes and with vybrant dye (50 nM Thermo Fisher Scientific) for nuclei for 30 min. Cell membranes were stained with cell mask deep red (Thermo Fisher Scientific) for 5 min before image acquisition. Samples were maintained at 37 °C with a 5% CO_2 using a stage-top incubator. Images were obtained using an oil objective on an SP8 Leica confocal microscope. All samples were monitored up to 6 h.

In Vivo Immunization Study. Balb/c mice were intramuscularly injected 20 μg OVA with NS-TLR, a mixture of 1V209 and silica nanoshells, unconjugated 1V209, or silica nanoshells on days 0 and 20. The mice intraperitoneally received 100 μg OVA on day 39. Mice were sacrificed on day 42, and the sera and spleens were collected. Sera were analyzed with IgG1 and IgG2a by ELISA. Splenocytes were cultured with OVA (100 μg/mL) in RP-10 for 5 days at 37 °C, and IFN-γ in the supernatant was determined by ELISA.

Statistical Analysis. One-way ANOVA with Tukey's post hoc test was employed to compare two or more groups. To compare cross-sectional outcomes among two or more groups, one-way ANOVA with Dunn's post hoc test was applied. $p < 0.05$ was considered statistically significant and denoted as $^*p < 0.05$, $^{**}p < 0.01$, and $^{***}p < 0.001$.

DOI: 10.1021/acsami.9b08295
ACS Appl. Mater. Interfaces 2019, 11, 26637−26647

■ ASSOCIATED CONTENT

Supporting Information

The Supporting Information is available free of charge on the ACS Publications website at DOI: 10.1021/acsami.9b08295.

Transmission electron microscopy images, ligand quantification, and drug potency of NS-TLR; IL-1β stimulation by silica nanoparticles (PDF)

■ AUTHOR INFORMATION

Corresponding Authors

*E-mail: thayashi@ucsd.edu (T.H.).
*E-mail: akummel@ucsd.edu (A.C.K.).

ORCID

Ching-Hsin Huang: 0000-0002-8396-3878
William C. Trogler: 0000-0001-6098-7685
Andrew C. Kummel: 0000-0001-8301-9855

Author Contributions

‖C.-H.H. and N.M. are co-first authors.

Funding

This study was funded by the National Institute of Health 611 grants U54CA132379, 5T32CA153915, and ViewPoint Medical Inc. Andrew Kummel and William Trogler are scientific advisors and have an equity interest in ViewPoint Medical Inc. The terms of this arrangement have been reviewed and approved by the University of California, San Diego, in accordance with its conflict of interest policies.

Notes

The authors declare the following competing financial interest(s): This study was funded by National Institute of Health grants U54CA132379 and ViewPoint Medical Inc. Andrew Kummel and William Trogler are scientific advisors and have an equity interest in ViewPoint Medical Inc. The terms of this arrangement have been reviewed and approved by the University of California, San Diego in accordance with its conflict of interest policies.

■ REFERENCES

(1) Fromen, C. A.; Rahhal, T. B.; Robbins, G. R.; Kai, M. P.; Shen, T. W.; Luft, J. C.; DeSimone, J. M. Nanoparticle Surface Charge Impacts Distribution, Uptake and Lymph Node Trafficking by Pulmonary Antigen-Presenting Cells. *Nanomedicine* **2016**, *12*, 677−687.

(2) Pradhan, P.; Qin, H.; Leleux, J. A.; Gwak, D.; Sakamaki, I.; Kwak, L. W.; Roy, K. The Effect of Combined IL10 SiRNA and CpG ODN as Pathogen-Mimicking Microparticles on Th1/Th2 Cytokine Balance in Dendritic Cells and Protective Immunity against B Cell Lymphoma. *Biomaterials* **2014**, *35*, 5491−5504.

(3) Xia, Y.; Wu, J.; Du, Y.; Miao, C.; Su, Z.; Ma, G. Bridging Systemic Immunity with Gastrointestinal Immune Responses via Oil-in-Polymer Capsules. *Adv. Mater.* **2018**, *30*, No. 1801067.

(4) Zhu, G.; Lynn, G. M.; Jacobson, O.; Chen, K.; Liu, Y.; Zhang, H.; Ma, Y.; Zhang, F.; Tian, R.; Ni, Q.; Cheng, S.; Wang, Z. Z.; Lu, N.; Yung, B. C.; Wang, Z. Z.; Lang, L.; Fu, X.; Jin, A.; Weiss, I. D.; Vishwasrao, H.; Niu, G.; Shroff, H.; Klinman, D. M.; Seder, R. A.; Chen, X. Albumin/Vaccine Nanocomplexes That Assemble in Vivo for Combination Cancer Immunotherapy. *Nat. Commun.* **2017**, *8*, No. 1954.

(5) Smirnov, D.; Schmidt, J. J.; Capecchi, J. T.; Wightman, P. D. Vaccine Adjuvant Activity of 3M-052: An Imidazoquinoline Designed for Local Activity without Systemic Cytokine Induction. *Vaccine* **2011**, *29*, 5434−5442.

(6) Lynn, G. M.; Laga, R.; Darrah, P. A.; Ishizuka, A. S.; Balaci, A. J.; Dulcey, A. E.; Pechar, M.; Pola, R.; Gerner, M. Y.; Yamamoto, A.; Buechler, C. R.; Quinn, K. M.; Smelkinson, M. G.; Vanek, O.; Cawood, R.; Hills, T.; Vasalatiy, O.; Kastenmüller, K.; Francica, J. R.; Stutts, L.; Tom, J. K.; Ryu, K. A.; Esser-Kahn, A. P.; Etrych, T.; Fisher, K. D.; Seymour, L. W.; Seder, R. A. In Vivo Characterization of the Physicochemical Properties of Polymer-Linked TLR Agonists That Enhance Vaccine Immunogenicity. *Nat. Biotechnol.* **2015**, *33*, 1201−1210.

(7) Li, C.; Zhang, X.; Chen, Q.; Zhang, J.; Li, W.; Hu, H.; Zhao, X.; Qiao, M.; Chen, D. Synthetic Polymeric Mixed Micelles Targeting Lymph Nodes Trigger Enhanced Cellular and Humoral Immune Responses. *ACS Appl. Mater. Interfaces* **2018**, *10*, 2874−2889.

(8) Shinchi, H.; Crain, B.; Yao, S.; Chan, M.; Zhang, S. S.; Ahmadiiveli, A.; Suda, Y.; Hayashi, T.; Cottam, H. B.; Carson, D. A. Enhancement of the Immunostimulatory Activity of a TLR7 Ligand by Conjugation to Polysaccharides. *Bioconjugate Chem.* **2015**, *26*, 1713−1723.

(9) Shao, K.; Singha, S.; Clemente-Casares, X.; Tsai, S.; Yang, Y.; Santamaria, P. Nanoparticle-Based Immunotherapy for Cancer. *ACS Nano* **2014**, *9*, 16−30.

(10) Knutson, K. L.; Disis, M. L. Tumor Antigen-Specific T Helper Cells in Cancer Immunity and Immunotherapy. *Cancer Immunol. Immunother.* **2005**, *54*, 721−728.

(11) Maisonneuve, C.; Bertholet, S.; Philpott, D. J.; De Gregorio, E. Unleashing the Potential of NOD-and Toll-like Agonists as Vaccine Adjuvants. *Proc. Natl. Acad. Sci. U.S.A.* **2014**, *111*, 12294−12299.

(12) Schön, M. P.; Schön, M. TLR7 and TLR8 as Targets in Cancer Therapy. *Oncogene* **2008**, *27*, 190−199.

(13) Walsh, K. B.; Teijaro, J. R.; Zuniga, E. I.; Welch, M. J.; Fremgen, D. M.; Blackburn, S. D.; von Tiehl, K. F.; Wherry, E. J.; Flavell, R. A.; Oldstone, M. B. A. Toll-like Receptor 7 Is Required for Effective Adaptive Immune Responses That Prevent Persistent Virus Infection. *Cell Host Microbe* **2012**, *11*, 643−653.

(14) Dumitru, C. D.; Antonysamy, M. A.; Tomai, M. A.; Lipson, K. E. Potentiation of the Anti-Tumor Effects of Imidazoquinoline Immune Response Modifiers by Cyclophosphamide. *Cancer Biol. Ther.* **2010**, *10*, 155−165.

(15) Latz, E.; Xiao, T. S.; Stutz, A. Activation and Regulation of the Inflammasomes. *Nat. Rev. Immunol.* **2013**, *13*, 397−411.

(16) Conniot, J.; Silva, J. M.; Fernandes, J. G.; Silva, L. C.; Gaspar, R.; Brocchini, S.; Florindo, H. F.; Barata, T. S. Cancer Immunotherapy: Nanodelivery Approaches for Immune Cell Targeting and Tracking. *Front. Chem.* **2014**, *2*, 105.

(17) Tao, C.; Zhu, Y.; Xu, Y.; Zhu, M.; Morita, H.; Hanagata, N. Mesoporous Silica Nanoparticles for Enhancing the Delivery Efficiency of Immunostimulatory DNA Drugs. *Dalton Trans.* **2014**, *43*, 5142−5150.

(18) Warashina, S.; Nakamura, T.; Sato, Y.; Fujiwara, Y.; Hyodo, M.; Hatakeyama, H.; Harashima, H. A Lipid Nanoparticle for the Efficient Delivery of SiRNA to Dendritic Cells. *J. Controlled Release* **2016**, *225*, 183−191.

(19) Rosalia, R. A.; Cruz, L. J.; van Duikeren, S.; Tromp, A. T.; Silva, A. L.; Jiskoot, W.; de Gruijl, T.; Löwik, C.; Oostendorp, J.; van der Burg, S. H.; Ossendorp, F. CD40-Targeted Dendritic Cell Delivery of PLGA-Nanoparticle Vaccines Induce Potent Anti-Tumor Responses. *Biomaterials* **2015**, *40*, 88−97.

(20) Sercombe, L.; Veerati, T.; Moheimani, F.; Wu, S. Y.; Sood, A. K.; Hua, S. Advances and Challenges of Liposome Assisted Drug Delivery. *Front. Pharmacol.* **2015**, *6*, 286.

(21) Narang, A.; Chang, R.-K.; Hussain, M. A. Pharmaceutical Development and Regulatory Considerations for Nanoparticles and Nanoparticulate Drug Delivery Systems. *J. Pharm. Sci.* **2013**, *102*, 3867−3882.

(22) Kaur, R.; Bramwell, V. W.; Kirby, D. J.; Perrie, Y. Pegylation of DDA:TDB Liposomal Adjuvants Reduces the Vaccine Depot Effect and Alters the Th1/Th2 Immune Responses. *J. Controlled Release* **2012**, *158*, 72−77.

(23) Kaur, R.; Henriksen-Lacey, M.; Wilkhu, J.; Devitt, A.; Christensen, D.; Perrie, Y. Effect of Incorporating Cholesterol into

DOI: 10.1021/acsami.9b08295
ACS Appl. Mater. Interfaces 2019, 11, 26637−26647

DDA:TDB Liposomal Adjuvants on Bilayer Properties, Biodistribution, and Immune Responses. *Mol. Pharmaceutics* **2013**, 197−207.
(24) Nakano, Y.; Mori, M.; Yamamura, H.; Naito, S.; Kato, H.; Taneichi, M.; Tanaka, Y.; Komuro, K.; Uchida, T. Cholesterol Inclusion in Liposomes Affects Induction of Antigen-Specific IgG and IgE Antibody Production in Mice by a Surface-Linked Liposomal Antigen. *Bioconjugate Chem.* **2002**, *13*, 744−749.
(25) Mahmud, M.; Piwoni, A.; Filiczak, N.; Janicka, M.; Gubernator, J. Long-Circulating Curcumin-Loaded Liposome Formulations with High Incorporation Efficiency, Stability and Anticancer Activity towards Pancreatic Adenocarcinoma Cell Lines In Vitro. *PLoS One* **2016**, *11*, No. e0167787.
(26) Koide, H.; Asai, T.; Hatanaka, K.; Akai, S.; Ishii, T.; Kenjo, E.; Ishida, T.; Kiwada, H.; Tsukada, H.; Oku, N. T Cell-Independent B Cell Response Is Responsible for ABC Phenomenon Induced by Repeated Injection of PEGylated Liposomes. *Int. J. Pharm.* **2010**, *392*, 218−223.
(27) Raghuvanshi, R. S.; Katare, Y. K.; Lalwani, K.; Ali, M. M.; Singh, O.; Panda, A. K. Improved Immune Response from Biodegradable Polymer Particles Entrapping Tetanus Toxoid by Use of Different Immunization Protocol and Adjuvants. *Int. J. Pharm.* **2002**, *245*, 109−121.
(28) Skwarczynski, M.; Toth, I. Peptide-Based Synthetic Vaccines. *Chem. Sci.* **2016**, *7*, 842−854.
(29) Desai, N. Challenges in Development of Nanoparticle-Based Therapeutics. *AAPS J.* **2012**, *14*, 282−295.
(30) Heidegger, S.; Gößl, D.; Schmidt, A.; Niedermayer, S.; Argyo, C.; Endres, S.; Bein, T.; Bourquin, C. Immune Response to Functionalized Mesoporous Silica Nanoparticles for Targeted Drug Delivery. *Nanoscale* **2016**, *8*, 938−948.
(31) Wang, X.; Li, X.; Ito, A.; Yoshiyuki, K.; Sogo, Y.; Watanabe, Y.; Yamazaki, A.; Ohno, T.; Tsuji, N. M. Hollow Structure Improved Anti-Cancer Immunity of Mesoporous Silica Nanospheres In Vivo. *Small* **2016**, *12*, 3510−3515.
(32) Wang, X.; Li, X.; Ito, A.; Watanabe, Y.; Sogo, Y.; Tsuji, N. M.; Ohno, T. Stimulation of in Vivo Antitumor Immunity with Hollow Mesoporous Silica Nanospheres. *Angew. Chem., Int. Ed.* **2016**, *55*, 1899−1903.
(33) Lu, Y.; Yang, Y.; Gu, Z.; Zhang, J.; Song, H.; Xiang, G.; Yu, C. Glutathione-Depletion Mesoporous Organosilica Nanoparticles as a Self-Adjuvant and Co-Delivery Platform for Enhanced Cancer Immunotherapy. *Biomaterials* **2018**, *175*, 82−92.
(34) Skrastina, D.; Petrovskis, I.; Lieknina, I.; Bogans, J.; Renhofa, R.; Ose, V.; Dishlers, A.; Dekhtyar, Y.; Pumpens, P. Silica Nanoparticles as the Adjuvant for the Immunisation of Mice Using Hepatitis B Core Virus-Like Particles. *PLoS One* **2014**, *9*, No. e114006.
(35) Hirai, T.; Yoshikawa, T.; Nabeshi, H.; Yoshida, T.; Tochigi, S.; Ichihashi, K.; Uji, M.; Akase, T.; Nagano, K.; Abe, Y.; Kamada, H.; Itoh, N.; Tsunoda, S.; Yoshioka, Y.; Tsutsumi, Y. Amorphous Silica Nanoparticles Size-Dependently Aggravate Atopic Dermatitis-like Skin Lesions Following an Intradermal Injection. *Part. Fibre Toxicol.* **2012**, *9*, 3.
(36) Martinez, H. P.; Kono, Y.; Blair, S. L.; Sandoval, S.; Wang-Rodriguez, J.; Mattrey, R. F.; Kummel, A. C.; Trogler, W. C. Hard Shell Gas-Filled Contrast Enhancement Particles for Colour Doppler Ultrasound Imaging of Tumors. *MedChemComm* **2010**, *1*, 266−270.
(37) Chan, M.; Hayashi, T.; Kuy, C. S.; Gray, C. S.; Wu, C. C. N.; Corr, M.; Wrasidlo, W.; Cottam, H. B.; Carson, D. A. Synthesis and Immunological Characterization of Toll-Like Receptor 7 Agonistic Conjugates. *Bioconjugate Chem.* **2009**, *20*, 1194−1200.
(38) Vallhov, H.; Gabrielsson, S.; Strømme, M.; Scheynius, A.; Garcia-Bennett, A. E. Mesoporous Silica Particles Induce Size Dependent Effects on Human Dendritic Cells. *Nano Lett.* **2007**, *7*, 3576−3582.
(39) Chang, J.-S.; Chang, K. L. B.; Hwang, D. F.; Kong, Z. L. In Vitro Cytotoxicitiy of Silica Nanoparticles at High Concentrations Strongly Depends on the Metabolic Activity Type of the Cell Line. *Environ. Sci. Technol.* **2007**, *41*, 2064−2068.
(40) Fubini, B.; Hubbard, A. Reactive Oxygen Species (ROS) and Reactive Nitrogen Species (RNS) Generation by Silica in Inflammation and Fibrosis. *Free Radical Biol. Med.* **2003**, *34*, 1507−1516.
(41) Chen, L.; Liu, J.; Zhang, Y.; Zhang, G.; Kang, Y.; Chen, A.; Feng, X.; Shao, L. The Toxicity of Silica Nanoparticles to the Immune System. *Nanomedicine* **2018**, *13*, 1939−1962.
(42) Lehman, S. E.; Morris, A. S.; Mueller, P. S.; Salem, A. K.; Grassian, V. H.; Larsen, S. C. Silica Nanoparticle-Generated ROS as a Predictor of Cellular Toxicity: Mechanistic Insights and Safety by Design. *Environ. Sci. Nano* **2016**, *3*, 56−66.
(43) Tanaka, T.; Narazaki, M.; Kishimoto, T. IL-6 in Inflammation, Immunity, and Disease. *Cold Spring Harbor Perspect. Biol.* **2014**, *6*, No. a016295.
(44) Tomić, S.; Đokić, J.; Vasilijić, S.; Ogrinc, N.; Rudolf, R.; Pelicon, P.; Vučević, D.; Milosavljević, P.; Janković, S.; Anžel, I.; Rajković, J.; Rupnik, M. S.; Friedrich, B.; Čolić, M. Size-Dependent Effects of Gold Nanoparticles Uptake on Maturation and Antitumor Functions of Human Dendritic Cells In Vitro. *PLoS One* **2014**, *9*, No. e96584.
(45) Seydoux, E.; Rothen-Rutishauser, B.; Nita, I. M.; Balog, S.; Gazdhar, A.; Stumbles, P. A.; Petri-Fink, A.; Blank, F.; von Garnier, C. Size-Dependent Accumulation of Particles in Lysosomes Modulates Dendritic Cell Function through Impaired Antigen Degradation. *Int. J. Nanomed.* **2014**, *9*, 3885−3902.
(46) Yang, J.; Lind, J. U.; Trogler, W. C. Synthesis of Hollow Silica and Titania Nanospheres. *Chem. Mater.* **2008**, *20*, 2875−2877.
(47) Bouvier, N. M.; Palese, P. The Biology of Influenza Viruses. *Vaccine* **2008**, *26*, D49−D53.
(48) Zhang, H.; Dunphy, D. R.; Jiang, X.; Meng, H.; Sun, B.; Tarn, D.; Xue, M.; Wang, X.; Lin, S.; Ji, Z.; Li, R.; Garcia, F. L.; Yang, J.; Kirk, M. L.; Xia, T.; Zink, J. I.; Nel, A.; Brinker, C. J. Processing Pathway Dependence of Amorphous Silica Nanoparticle Toxicity: Colloidal vs Pyrolytic. *J. Am. Chem. Soc.* **2012**, *134*, 15790−15804.
(49) Hornung, V.; Bauernfeind, F.; Halle, A.; Samstad, E. O.; Kono, H.; Rock, K. L.; Fitzgerald, K. A.; Latz, E. Silica Crystals and Aluminum Salts Activate the NALP3 Inflammasome through Phagosomal Destabilization. *Nat. Immunol.* **2008**, *9*, 847−856.
(50) Dostert, C.; Petrilli, V.; Van Bruggen, R.; Steele, C.; Mossman, B. T.; Tschopp, J. Innate Immune Activation Through Nalp3 Inflammasome Sensing of Asbestos and Silica. *Science* **2008**, *320*, 674−677.
(51) Morishige, T.; Yoshioka, Y.; Inakura, H.; Tanabe, A.; Yao, X.; Narimatsu, S.; Monobe, Y.; Imazawa, T.; Tsunoda, S.; Tsutsumi, Y.; Mukai, Y.; Okada, N.; Nakagawa, S. The Effect of Surface Modification of Amorphous Silica Particles on NLRP3 Inflammasome Mediated IL-1β Production, ROS Production and Endosomal Rupture. *Biomaterials* **2010**, *31*, 6833−6842.
(52) Sandberg, W. J.; Låg, M.; Holme, J. A.; Friede, B.; Gualtieri, M.; Kruszewski, M.; Schwarze, P. E.; Skuland, T.; Refsnes, M. Comparison of Non-Crystalline Silica Nanoparticles in IL-1β Release from Macrophages. *Part. Fibre Toxicol.* **2012**, *9*, 32.
(53) Al Moussawi, K.; Kazmierczak, B. I. Distinct Contributions of Interleukin-1α (IL-1α) and IL-1β to Innate Immune Recognition of *Pseudomonas aeruginosa* in the Lung. *Infect. Immun.* **2014**, *82*, 4204−4211.
(54) Newton, K.; Dixit, V. M. Signaling in Innate Immunity and Inflammation. *Cold Spring Harbor Perspect. Biol.* **2012**, *4*, No. a006049.
(55) Castellani, P.; Rubartelli, A.; Lavieri, R.; Piccioli, P.; Carta, S.; Delfino, L. Anti-Inflammatory Cytokine Production with Unbalance of Proinflammatory and TLR Costimulation Causes Oxidative Stress. *J. Immunol.* **2019**, *192*, 5373−5381.
(56) He, Y.; Hara, H.; Núñez, G. Mechanism and Regulation of NLRP3 Inflammasome Activation. *Trends Biochem. Sci.* **2016**, *41*, 1012−1021.
(57) Davis, B. K.; Wen, H.; Ting, J. P.-Y. The Inflammasome NLRs in Immunity, Inflammation, and Associated Diseases. *Annu. Rev. Immunol.* **2011**, *29*, 707−735.

DOI: 10.1021/acsami.9b08295
ACS Appl. Mater. Interfaces 2019, 11, 26637−26647

(58) Ghiringhelli, F.; Apetoh, L.; Tesniere, A.; Aymeric, L.; Ma, Y.; Ortiz, C.; Vermaelen, K.; Panaretakis, T.; Mignot, G.; Ullrich, E.; Perfettini, J.-L.; Schlemmer, F.; Tasdemir, E.; Uhl, M.; Génin, P.; Civas, A.; Ryffel, B.; Kanellopoulos, J.; Tschopp, J.; André, F.; Lidereau, R.; McLaughlin, N. M.; Haynes, N. M.; Smyth, M. J.; Kroemer, G.; Zitvogel, L. Activation of the NLRP3 Inflammasome in Dendritic Cells Induces IL-1β−Dependent Adaptive Immunity against Tumors. *Nat. Med.* **2009**, *15*, 1170−1178.
(59) Russell, R. F.; McDonald, J. U.; Lambert, L.; Tregoning, J. S. Use of the Microparticle Nanoscale Silicon Dioxide as an Adjuvant To Boost Vaccine Immune Responses against Influenza Virus in Neonatal Mice. *J. Virol.* **2016**, *90*, 4735−4744.
(60) Holdsworth, S. R.; Kitching, A. R.; Tipping, P. G. Th1 and Th2 T Helper Cell Subsets Affect Patterns of Injury and Outcomes in Glomerulonephritis. *Kidney Int.* **1999**, *55*, 1198−1216.
(61) Spellberg, B.; Edwards, J. E. Type 1/Type 2 Immunity in Infectious Diseases. *Clin. Infect. Dis.* **2001**, *32*, 76−102.
(62) Eisenbarth, S. C.; Colegio, O. R.; O'Connor, W.; Sutterwala, F. S.; Flavell, R. A. Crucial Role for the Nalp3 Inflammasome in the Immunostimulatory Properties of Aluminium Adjuvants. *Nature* **2008**, *453*, 1122−1126.
(63) Wen, Y.; Shi, Y. Alum: An Old Dog with New Tricks. *Emerging Microbes Infect.* **2016**, *5*, 1−5.
(64) Lee, S.; Nguyen, M. T. Recent Advances of Vaccine Adjuvants for Infectious Diseases. *Immune Netw.* **2015**, *15*, 51−57.
(65) Buonsanti, C.; Balocchi, C.; Harfouche, C.; Corrente, F.; Galli Stampino, L.; Mancini, F.; Tontini, M.; Malyala, P.; Bufali, S.; Baudner, B.; De Gregorio, E.; Valiante, N. M.; O'Hagan, D. T.; Rappuoli, R.; D'Oro, U. Novel Adjuvant Alum-TLR7 Significantly Potentiates Immune Response to Glycoconjugate Vaccines. *Sci. Rep.* **2016**, *6*, No. 29063.
(66) Gherardi, R. K.; Eidi, H.; Crépeaux, G.; Authier, F. J.; Cadusseau, J. Biopersistence and Brain Translocation of Aluminum Adjuvants of Vaccines. *Front. Neurol.* **2015**, *6*, 4.
(67) Liberman, A.; Mendez, N.; Trogler, W. C.; Kummel, A. C. Synthesis and Surface Functionalization of Silica Nanoparticles for Nanomedicine. *Surf. Sci. Rep.* **2014**, *69*, 132−158.
(68) Suthabanditpong, W.; Takai, C.; Fuji, M.; Buntem, R.; Shirai, T. Improved Optical Properties of Silica/UV-Cured Polymer Composite Films Made of Hollow Silica Nanoparticles with a Hierarchical Structure for Light Diffuser Film Applications. *Phys. Chem. Chem. Phys.* **2016**, *18*, 16293−16301.
(69) Weigand, R.; F. Rotermund, A.; Penzkofer, A. Aggregation Dependent Absorption Reduction of Indocyanine Green. *J. Phys. Chem. A* **1997**, *101*, 7729−7734.
(70) Hayashi, T.; Rao, S. P.; Takabayashi, K.; Van Uden, J. H.; Kornbluth, R. S.; Baird, S. M.; Taylor, M. W.; Carson, D. A.; Catanzaro, A.; Raz, E. Enhancement of Innate Immunity against Mycobacterium Avium Infection by Immunostimulatory DNA Is Mediated by Indoleamine 2,3-Dioxygenase. *Infect. Immun.* **2001**, *69*, 6156−6164.

DOI: 10.1021/acsami.9b08295
ACS Appl. Mater. Interfaces 2019, 11, 26637−26647